Helmholtz-Zentrum Dresden-Rossendorf (HZDR)

HELMHOLTZ ZENTRUM
DRESDEN ROSSENDORF

Unified modeling of bubbly flows in pipes, bubble columns, and airlift columns

Rzehak, R.; Ziegenhein, T.; Kriebitzsch, S.; Krepper, E.; Lucas, D.;

Originally published:

May 2016

Chemical Engineering Science 157(2017), 147-158

DOI: https://doi.org/10.1016/j.ces.2016.04.056

Perma-Link to Publication Repository of HZDR:

https://www.hzdr.de/publications/Publ-22634

Release of the secondary publication
on the basis of the German Copyright Law § 38 Section 4.

CC BY-NC-ND

Author's Accepted Manuscript

Unified modeling of bubbly flows in pipes, bubble columns, and airlift columns

Roland Rzehak, Thomas Ziegenhein, Sebastian Kriebitzsch, Eckhard Krepper, Dirk Lucas

Chemical Engineering Science

www.elsevier.com/locate/ces

PII: S0009-2509(16)30222-6
DOI: http://dx.doi.org/10.1016/j.ces.2016.04.056
Reference: CES12934

To appear in: *Chemical Engineering Science*

Received date: 17 September 2015
Revised date: 11 April 2016
Accepted date: 29 April 2016

Cite this article as: Roland Rzehak, Thomas Ziegenhein, Sebastian Kriebitzsch Eckhard Krepper and Dirk Lucas, Unified modeling of bubbly flows in pipes bubble columns, and airlift columns, *Chemical Engineering Science* http://dx.doi.org/10.1016/j.ces.2016.04.056

This is a PDF file of an unedited manuscript that has been accepted fo publication. As a service to our customers we are providing this early version o the manuscript. The manuscript will undergo copyediting, typesetting, an review of the resulting galley proof before it is published in its final citable form Please note that during the production process errors may be discovered whic could affect the content, and all legal disclaimers that apply to the journal pertain

ACCEPTED MANUSCRIPT

Unified modeling of bubbly flows in pipes, bubble columns, and airlift columns

Roland Rzehak*, Thomas Ziegenhein, Sebastian Kriebitzsch, Eckhard Krepper, Dirk Lucas

Helmholtz-Zentrum Dresden - Rossendorf, Institute of Fluid Dynamics, P.O. Box 510119 D-01314 Dresden, Germany

*Corresponding author. r.rzehak@hzdr.de

Abstract

Multiphase CFD simulation is a valuable tool in process engineering which is particularly useful to study new reactor concepts and their scale-up from laboratory to production scale. Simulations of bubbly flows up to industrial dimensions are feasible within the Eulerian two-fluid framework of interpenetrating continua. However, for practical applications suitable closure models are needed which describe the physics on the scale of individual bubbles or groups thereof. The quest for such models with a broad range of applicability allowing predictive simulations is an ongoing venture.

A set of closure relations for the fluid dynamics of bubbly flow has been collected that represents the best available knowledge and may serve as a baseline for further improvements and extensions. It is shown that this model is applicable to bubbly flows in different systems, namely pipes, bubble columns, and airlift columns. While some of these systems have been considered individually before, the novelty of the present work lies in their unified treatment by a single model.

Keywords: dispersed gas-liquid multiphase flow, Euler-Euler two-fluid model, closure relations, CFD simulation, model validation, pipe flow, bubble column, airlift column

1 INTRODUCTION

The purpose of computer-aided process engineering (CAPE) is to assist the development and operation of complex processes involving chemical or physical change (Joshi and Ranade 2003). Computational fluid dynamics (CFD) simulations are a means to study in detail unit operations, such as mixing, reaction, separation or combinations thereof, performed in a specific type of equipment. In particular scale-up studies and the evaluation of concepts for process intensification in an early design phase promise high benefits in terms of identifying energy- and resource-efficient solutions which are expensive to assess by conventional semi-empirical methods (Ranade 1995, Sundaresan 2000, Joshi 2001, Jakobsen et al. 2005, Dudukovic 2010).

CFD simulations of dispersed bubbly flow on the scale of technical equipment are feasible within the Eulerian two-fluid framework of interpenetrating continua. However, accurate numerical predictions rely on suitable closure models describing the physics on the scale of individual bubbles or groups thereof. A large number of works exists, in each of which largely a different set of closure relations is compared to a different set of experimental data. For the limited range of conditions to which each model variant is applied, reasonable agreement with the data is mostly obtained, but due to a lack of comparability between the individual works no complete, reliable, and robust formulation has emerged so far. Moreover, the models usually contain a number of empirical parameters that have been adjusted to match the particular data that were used in the comparison. Predictive simulation, however, requires a model that works without any adjustments within the targeted domain of applicability.

Accepted manuscript

ACCEPTED MANUSCRIPT

As a step towards this goal, an attempt has been made to collect the best available description for all aspects known to be relevant for adiabatic bubbly flows in which only momentum is exchanged between liquid and gas phases. Apart from interest in its own right, results obtained for this restricted problem also provide a good starting point for the investigation of more complex situations including heat and mass transport, phase change, and chemical reactions.

Aspects requiring closure for the case under consideration are: (i) the exchange of momentum between liquid and gas phases, (ii) the effects of the dispersed bubbles on the turbulence of the liquid carrier phase, and (iii) processes of bubble coalescence and breakup that determine the distribution of bubble sizes. All of these aspects are coupled and therefore in principle have to be considered as a whole.

At the same time it is highly desirable to validate the individual sub-models of this complex coupled problem separately. To this end we use a step-by-step procedure in which we first consider situations where a fixed distribution of bubble sizes may be imposed. In this way the sub-models for bubble forces (i) and bubble-induced turbulence (ii) can be validated independently of bubble coalescence and breakup processes (iii). The latter will be added later on in a second step building on the already established sub-models for the former.

In the present contribution the baseline model referred to above is applied to several different configurations commonly encountered in chemical engineering applications, namely bubbly flows in pipes, bubble columns, and airlift columns. Since in all of these systems the small scales are governed by the same physics it is expected that they can be treated in a unified manner using the same set of closure relations. By comparison of simulation results to experimental data taken from the literature this is shown to be the case within a certain accuracy and the model is validated for all of these configurations.

In this way a starting point for the prediction of flow phenomena is obtained. Expanding the range of applicability as well as the achieved accuracy is a continuously ongoing development effort. From the observed level of agreement between simulation and experiment issues requiring further investigation can be identified. This includes both the need for further model development and the need for CFD-grade experimental investigations.

2 DESCRIPTION OF THE BASELINE MODEL

The conservation equations of the Euler-Euler two-fluid model have been discussed at length in a number of books (e.g. Drew and Passman 1998, Yeoh and Tu 2010, Ishii and Hibiki 2011), while the extension to treat multiple bubble size and velocity classes (inhomogeneous MUSIG model) have been presented in several research papers (e.g. Frank et al. 2008, Krepper et al. 2008). A broad consensus has been reached, so this general framework will not be repeated here. Closure relations required to complete the model, in contrast, are still subject to considerable variation between researchers. Here, the baseline model that has emerged from previous work (Rzehak et al. 2012, Rzehak and Krepper 2013a,b, Ziegenhein et al. 2015, Rzehak and Krepper 2015, Liao et al. 2016) is adopted. This model has been validated for a number of different test cases including bubbly flow in pipes and bubble columns. Details of the model are given in section 2.1 for the bubble forces and in section 2.2 for bubble-induced turbulence.

2.1 Bubble Forces

Concerning momentum exchange between liquid and gas phase we consider drag, virtual mass, lift, wall, and turbulent dispersion forces. The correlations are expressed in terms of the

ACCEPTED MANUSCRIPT

dimensionless numbers, namely the Reynolds number $Re = |u_G - u_L| d_B \nu_L^{-1}$, the Eötvös number $Eo = (\rho_L - \rho_G) g d_B^2 \sigma^{-1}$, and the Morton number $Mo = (\rho_L - \rho_G) \rho_L^2 g \nu_L^4 \sigma^{-3}$.

2.1.1 Drag Force

The drag force reflects the resistance opposing bubble motion relative to the surrounding liquid. The corresponding gas-phase momentum source is given by

$$\mathbf{F}^{drag} = -\frac{3}{4d_B} C_D \rho_L \alpha_G |\mathbf{u}_G - \mathbf{u}_L| \, (\mathbf{u}_G - \mathbf{u}_L) \ . \tag{2}$$

The drag coefficient C_D depends strongly on the Reynolds number Re and for deformable bubbles also on the Eötvös number Eo. A correlation distinguishing different shape regimes has been suggested by Ishii and Zuber (1979), namely

$$C_D = \max\left(C_{D,sphere}, \min\left(C_{D,ellipse}, C_{D,cap}\right)\right) , \tag{3}$$

where

$$\begin{aligned} C_{D,sphere} &= \frac{24}{\mathrm{Re}}\left(1 + 0.1 \ \mathrm{Re}^{0.75}\right) \\ C_{D,ellipse} &= \frac{2}{3}\sqrt{\mathrm{Eo}} \\ C_{D,cap} &= \frac{8}{3} \end{aligned} \quad . \tag{4}$$

This correlation was compared with an extensive data set on the terminal velocity of bubbles rising in quiescent liquids covering several orders of magnitude for each of Re, Eo and Mo in (Tomiyama et al. 1998) with good agreement except at high values of Eo.

2.1.2 Lift Force

A bubble moving in an unbounded shear flow experiences a force perpendicular to the direction of its motion. The momentum source corresponding to this shear lift force, often simply referred to as lift force, can be calculated as (Zun 1980):

$$F^{lift} = -C_L \rho_L \alpha_G (u_G - u_L) \times rot(u_L) , \tag{5}$$

For a spherical bubble the shear lift coefficient C_L is positive so that the lift force acts in the direction of decreasing liquid velocity, i.e. in case of co-current pipe flow in the direction towards the pipe wall. Experimental (Tomiyama et al. 2002) and numerical (Schmidtke 2008) investigations showed, that the direction of the lift force changes its sign if a substantial deformation of the bubble occurs. From the observation of the trajectories of single air bubbles rising in simple shear flow of a glycerol water solution the following correlation for the lift coefficient was derived:

Accepted manuscript

$$C_L = \begin{cases} \min[0.288\tanh(0.121\,\mathrm{Re}),\, f(Eo_\perp)] & Eo_\perp < 4 \\ f(Eo_\perp) & \text{for} \quad 4 < Eo_\perp < 10 \\ -0.27 & 10 < Eo_\perp \end{cases} . \qquad (6)$$

$$\text{with} \quad f(Eo_\perp) = 0.00105 Eo_\perp^3 - 0.0159 Eo_\perp^2 - 0.0204 Eo_\perp + 0.474$$

This coefficient depends on the modified Eötvös number given by

$$Eo_\perp = \frac{g(\rho_L - \rho_G) d_\perp^2}{\sigma}, \qquad (7)$$

where $d_\perp$ is the maximum horizontal dimension of the bubble. It is calculated using an empirical correlation for the aspect ratio by Wellek et al. (1966) with the following equation:

$$d_\perp = d_B \sqrt[3]{1 + 0.163\, Eo^{0.757}}, \qquad (8)$$

where Eo is the usual Eötvös number. The resulting bubble size dependence of the lift coefficient for air bubble in water is shown in Fig. 1 from which the change in sign is seen to occur at a bubble size of $d_B \approx 6$ mm.

The experimental conditions on which Eq. (6) is based, were limited to the range $-5.5 \le \log_{10} \mathrm{Mo} \le -2.8$, $1.39 \le \mathrm{Eo} \le 5.74$ and values of the Reynolds number based on bubble diameter and shear rate $0 \le \mathrm{Re} \le 10$. The water-air system at normal conditions has a Morton number $\mathrm{Mo} = 2.63 \cdot 10^{-11}$ which is quite different, but good results have nevertheless been reported for this case (Lucas and Tomiyama 2011).

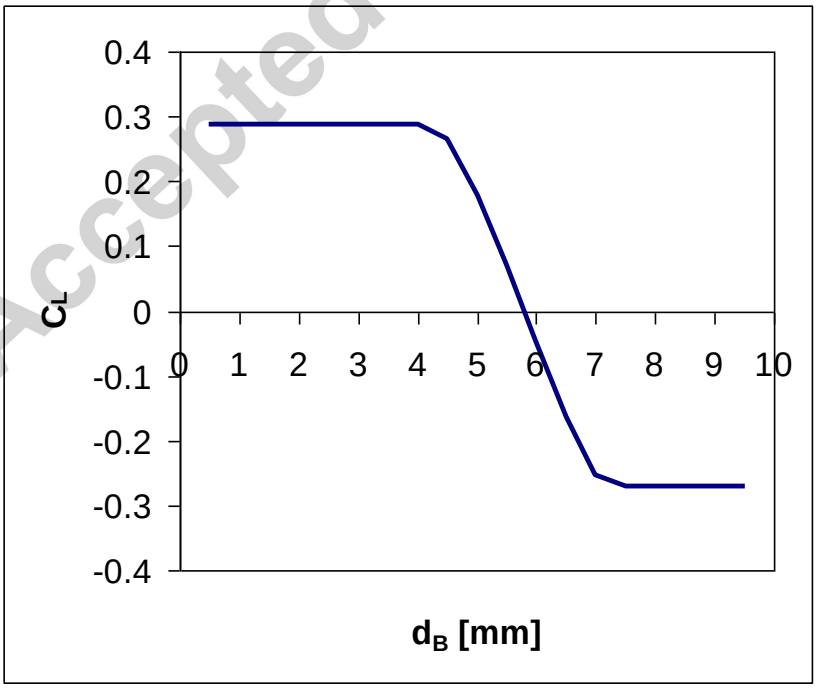

Accepted manuscript

ACCEPTED MANUSCRIPT

Figure 1: Dependence of the lift coefficient C_L on the bubble size d_B for air bubbles in water according to Eqs. (6) – (8).

2.1.3 Wall Force

A bubble translating next to a wall in an otherwise quiescent liquid also experiences a lift force. This wall lift force, often simply referred to as wall force, has the general form

$$\mathbf{F}^{wall} = \frac{2}{d_B} C_W \rho_L \alpha_G \left|\mathbf{u}_G - \mathbf{u}_L\right|^2 \hat{\mathbf{y}} \ , \tag{9}$$

where $\hat{\mathbf{y}}$ is the unit normal perpendicular to the wall pointing into the fluid. The dimensionless wall force coefficient C_W depends on the distance to the wall y and is expected to be positive, so the bubble is driven away from the wall.
Based on the observation of single bubble trajectories in simple shear flow of a glycerol water solution Tomiyama et al. (1995) and later Hosokawa et al. (2002) concluded a functional dependence

$$C_W(y) = f(Eo)\left(\frac{d_B}{2y}\right)^2 \ . \tag{10}$$

In the limit of small Morton number the correlation

$$f(Eo) = 0.0217 \ \ Eo \tag{11}$$

is derived from the data of Hosokawa et al. (2002). The experimental conditions which Eq. (11) is based on are $2.2 \le Eo \le 22$ and $-6.0 \le \log_{10} Mo \le -2.5$. This is still different from the water-air system with $Mo = 2.63 \cdot 10^{-11}$ but nonetheless a recent investigation (Rzehak et al. 2012) has nonetheless shown that good predictions are obtained also for air bubbles in water.

2.1.4 Turbulent Dispersion Force

The turbulent dispersion force describes the effect of the turbulent fluctuations of liquid velocity on the bubbles. Burns et al. (2004) derived an explicit expression by Favre averaging the drag force as:

$$\mathbf{F}^{disp} = -\frac{3}{4} C_D \frac{\alpha_G}{d_B} \left|\mathbf{u}_G - \mathbf{u}_L\right| \frac{\mu_L^{turb}}{\sigma_{TD}} \left(\frac{1}{\alpha_L} + \frac{1}{\alpha_G}\right) \mathrm{grad}\, \alpha_G \ . \tag{12}$$

In analogy to molecular diffusion, σ_{TD} is referred to as a Schmidt number. In principle it should be possible to obtain its value from single bubble experiments also for this force by evaluating the statistics of bubble trajectories in well characterized turbulent flows but to our knowledge this has not been done yet. A value of $\sigma_{TD} = 0.9$ is typically used.

Accepted manuscript

ACCEPTED MANUSCRIPT

In the same work the expression for the so-called Favre averaged drag (FAD) model has also been compared with other suggestions which all agree at least in the limit of low gas fraction.

2.1.5 Virtual Mass Force

When a bubble is accelerated, a certain amount of liquid has to be set into motion as well. This may be expressed as a force acting on the bubble as

$$\mathbf{F}^{VM} = -C_{VM}\rho_L\alpha_G\left(\frac{D_G\mathbf{u}_G}{Dt} - \frac{D_L\mathbf{u}_L}{Dt}\right), \tag{13}$$

where D_G / Dt and D_L / Dt denote material derivatives with respect to the velocity of the indicated phase. For the virtual mass coefficient a value of C_{VM} = 0.5 has been derived for isolated spherical bubbles in inviscid and creeping flows by Auton et al. (1988) and Maxey and Riley (1983), respectively. Results of direct simulations of a single bubble by Magnaudet et al. (1995) suggest that this value also holds for intermediate values of Re.

2.2 Two-phase Turbulence

Due to the small density and small spatial scales of the dispersed gas it suffices to consider turbulence in the continuous liquid phase for bubbly flows. We adopt a two equation turbulence model for the liquid phase with additional source terms describing bubble induced turbulence. The formulation given is equally applicable to either the k-ε, k-ω or SST model. Presently, the SST model will be used, since it combines advantages of the k-ω model near the walls and the k-ε model away from them as shown for single phase flows by Menter (1994, 2009) .
Concerning the source term describing bubble effects in the k-equation there is large agreement in the literature (e. g. Kataoka et al. 1992, Troshko and Hassan 2001). A plausible approximation is provided by the assumption that all energy lost by the bubble due to drag is converted to turbulent kinetic energy in the wake of the bubble. Hence, the k-source becomes

$$S_L^k = \mathbf{F}_L^{drag}\cdot\left(\mathbf{u}_G - \mathbf{u}_L\right). \tag{14}$$

For the ε-source a similar heuristic is used as for the single phase model, namely the k-source is divided by some time scale τ so that

$$S_L^\varepsilon = C_{\varepsilon B}\frac{S_L^k}{\tau}. \tag{15}$$

Further modeling then focuses on the time scale τ proceeding largely based on dimensional analysis. This follows the same line as the standard modeling of shear-induced turbulence in single phase flows (Wilcox 1998), where production terms in the ε-equation are obtained by multiplying corresponding terms in the k-equation by an appropriate time scale which represents the life-time of a turbulent eddy before it breaks up into smaller structures. In single phase turbulence the relevant variables are obviously k and ε from which only a single time scale $\tau = k_L/\varepsilon_L$ can be formed. For the bubble-induced turbulence in two-phase flows the situation is

ACCEPTED MANUSCRIPT

more complex. Obviously there are two length and two velocity scales in the problem, where one of each is related to the bubble and the other to the turbulent eddies. From these a total of four different time scales can be formed. In the absence of theoretical arguments to decide which of these is the most relevant one, a comparison of all four alternatives has shown the best performance for the choice $\tau = d_B / \sqrt{k_L}$ (Rzehak and Krepper 2013a) and this is followed herein. For the coefficient $C_{\varepsilon B}$ a value of 1.0 was found to give reasonable results.

For use with the SST model, the ε-source is transformed to an equivalent ω-source which gives

$$S_L^{\omega} = \frac{1}{C_{\mu} k_L} S_L^{\varepsilon} - \frac{\omega_L}{k_L} S_L^{k} \quad . \tag{16}$$

This ω-source is used independently of the blending function in the SST model since it should be effective throughout the fluid domain.

Since bubble-induced effects are included in k and ε / ω due to the respective source terms, the turbulent viscosity is evaluated from the standard formula

$$\mu_L^{turb} = C_{\mu} \rho_L \frac{{k_L}^2}{\varepsilon_L} \tag{17}$$

The effective viscosity is simply $\mu_L^{eff} = \mu_L^{mol} + \mu_L^{turb}$.

Boundary conditions on k and ε / ω are taken the same as for the single phase case, which is consistent with the view that the full wall shear stress is exerted by the liquid phase which contacts the full wall area. A single phase wall function is employed to avoid the need to resolve the viscous sublayer.

All turbulence model parameters take their usual single phase values for the presently investigated tests.

3 COMPARISON OF SIMULATION RESULTS AND EXPERIMENTAL DATA

Three different test cases have been selected form the literature where measurements suitable for model validation are available. These comprise bubbly flow in a round pipe (Liu 1998), a rectangular bubble column (bin Mohd Akbar et al. 2012), and a round airlift column with internal draft tube (Luo 2005). Length and lateral dimension of the test section vary as well as liquid and gas volumetric flow rates, J_L and J_G, average gas fraction, $\langle \alpha_G \rangle$, and average bubble size, $\langle d_B \rangle$. A summary of the relevant parameters is given in Table 1. Common to all tests is the use of air bubbles in water at ambient conditions.

Accepted manuscript

ACCEPTED MANUSCRIPT

Table1: Experimental conditions for all selected test cases.

name	D mm	J_L m/s	J_G m/s	$\langle d_B \rangle$ mm	$\langle \alpha_G \rangle$ %
Liu (1998): round pipe					
L21B	57.2	1.0	0.14	3.03	10.6
L21C	57.2	1.0	0.13	4.22	9.6
L22A	57.2	1.0	0.22	3.89	15.7
L11A	57.2	0.5	0.12	2.94	15.2
bin Mohd Akbar et al. (2012): flat bubble column					
A1	240	-	0.003	4.3	1.4
A2	240	-	0.013	5.5	6.2
Luo (2005): round airlift column					
	130	-	0.01	(3)	3.5

Simulations have been run using a customized version of ANSYS CFX. Different setups have been used making simplifications appropriate to the case at hand. Details will be given in the subsection for each case below. For all cases a high resolution scheme ensuring boundedness has been used to discretize the advective terms. For transient simulations a second order backwards Euler discretization was employed for the temporal discretization. The coupled solver option was chosen for the gas-fraction coupling. For further details we refer to the ANSYS CFX documentation (ANSYS, 2012).

A great speed up of the computation is achieved when planar or axisymmetric conditions are assumed so that it suffices to consider only a narrow slice or sector of the column. In that case the simulation may also be run in stationary mode. This approximation works well if large scale fluctuations are unimportant. Grid refinement studies were performed for all test cases to ensure sufficient resolution of the discretization. For all cases, coordinates are chosen such that the x-coordinate is along main flow direction and the z-or r-coordinate along the measured profiles.

For the inlet conditions a simplified treatment is possible when the measurements are made sufficiently far away such that fully developed flow conditions, which are not affected by the inlet conditions anymore, may be assumed there. The simplification consists in neglecting details of the gas supply and prescribing a uniform gas flux through the cross section of the domain or a portion thereof which is much larger than the dimensions of the sparger holes. In particular for pipe flow a truncation of the computational domain is unavoidable and fully developed single phase profiles may be used for the liquid velocity and turbulence quantities at the inlet.

On all solid walls a no-slip condition has been used for the liquid phase and a free-slip condition for the gas phase assuming that direct contacts between the bubbles and the walls are negligible. To avoid the need to resolve the viscous sublayer, a single phase turbulent wall function assuming a smooth wall has been applied.

Information on the bubble size is taken from the experimental data. To capture the different direction of motion for large and small bubbles according to the lift-force correlation of section 2.1.2, an inhomogeneous MUSIG model with two velocity groups is used for bubbles larger and smaller than 6 mm in size when needed. The contribution of each group to the total gas fraction is calculated from the measured bubble size distributions and kept fixed during the simulation. Therefore this treatment is referred to as fixed polydispersity. When only bubbles smaller than 6 mm exist, it reduces to the monodisperse approximation.

Air and water are treated as materials with constant properties at ambient conditions. Values used for the material properties are listed in Table 2.

Accepted manuscript

ACCEPTED MANUSCRIPT

Table 2: Material properties for the air water system at atmospheric pressure and 25°C temperature.

ρ_L	997.0	kg m^{-3}
μ_L	8.899e-4	kg m^{-1} s^{-1}
ρ_G	1.185	kg m^{-3}
μ_G	1.831e-05	kg m^{-1} s^{-1}
σ	0.072	N m^{-1}

Individual discussions of the results have been presented before (Rzehak and Krepper 2013, Ziegenhein et al. 2015, Liao et al. 2016). However put in the perspective of the present work, a new quality of insight is achieved. Thus some unavoidable repetition seems justified. Comparison of the different test cases shows that one and the same closure model for the small scale physics gives good agreement for quite different systems with various geometries and boundary conditions. This is an essential point for multiphase flow modelling using the Eulerian approach which may be expected intuitively but has not been demonstrated explicitly before.

3.1 Bubbly Pipe Flow Test Case

The system studied by Liu (1998) is a vertical upflow of water and air in a round pipe with inner diameter D = 57.2 mm, presumably at ambient conditions. The total length of the flow section was H = 3.43 m. A special gas injector was used that allowed to adjust the bubble size independently of liquid and gas volume fluxes. A variety of combinations of these three parameters are available. Radial profiles of gas-fraction, mean bubble size, axial liquid velocity, and axial liquid turbulence intensity were measured at an axial position L / D = 60 corresponding to fully developed conditions. A dual needle electrical conductivity probe was used to measure gas fraction and bubble size and a hot-film probe for liquid velocity and turbulence.

Four combinations of J_L, J_G, and d_B have been selected where the mean bubble size does not vary significantly over the pipe radius so that a monodisperse approximation is sensible. For comparison with the simulations and other test cases the axial liquid turbulence intensity is taken as a measure of the square root of turbulent kinetic energy. By considering the limits of isotropic and unidirectional turbulence the error incurred by this identification is estimated as $\sqrt{(1/2)}\ u' \le \sqrt{k} \le \sqrt{(3/2)}\ u'$.

Due to the significant variation of pressure within the domain, the gas density will change according to the ideal gas law and consequently the bubble size changes since mass is conserved. Yet the flow of both gas and liquid remains incompressible to a good approximation. To keep the computational advantage of treating both gas and liquid as incompressible fluids with constant material properties in a fully developed flow, as discussed in Rzehak et al. (2012), the gas flux at the inlet is adjusted to the value obtained by evaluating

Accepted manuscript

$$J_G = 2\pi \int_0^{D/2} \alpha_G(r)\, u_G(r)\, r\, dr \qquad (18)$$

using the data at the measurement location. For the tests of Liu (1998) only u_L but not u_G has been measured, so an estimate of the latter may be obtained from the former and α_G based on the assumption of fully developed stationary flow. The adjusted values resulting from this procedure are given in Table 1.

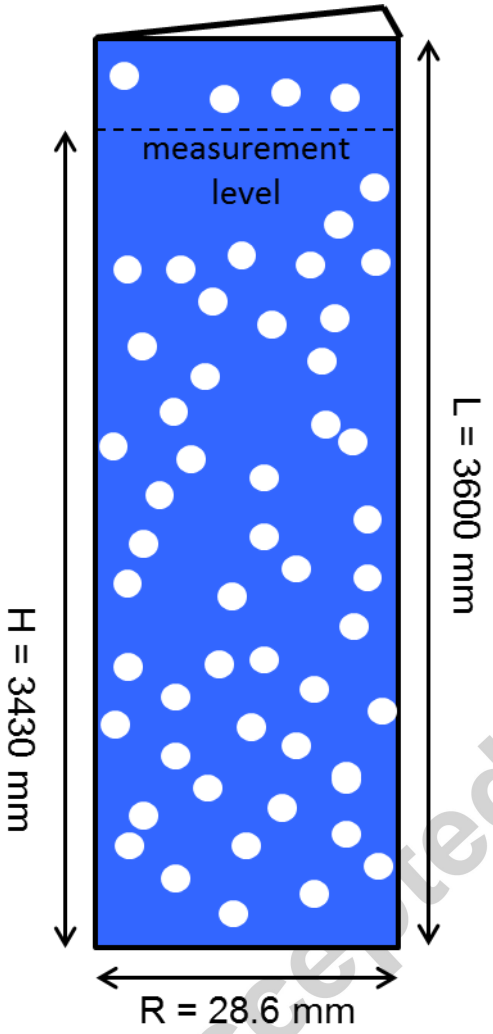

Figure 2: Sketch of the computational domain for the test cases of Liu (1998).

A sketch of the geometry used for the simulations is shown in Fig. 2. Based on the assumption of axisymmetric flow the domain was reduced to a narrow sector of the pipe with symmetry conditions imposed on the side faces and the simulations were run in stationary mode. At the beginning of the test section the profiles for the liquid flow were set according to a typical single phase turbulent flow profile in a pipe as an inlet condition. Gas volume fraction and mass flux are set to uniform values at the inlet. After the measurement location a flow abatement zone with a length of ~5% of the main flow section was added to ensure that there is no influence of the outlet condition imposed at the top of the domain. A pressure boundary condition was set at the top. The grid spacing was 0.715 mm in the radial and 5.55

Accepted manuscript

mm in the axial direction. Since the simulations were run in stationary mode, no time-step needs to be prescribed.

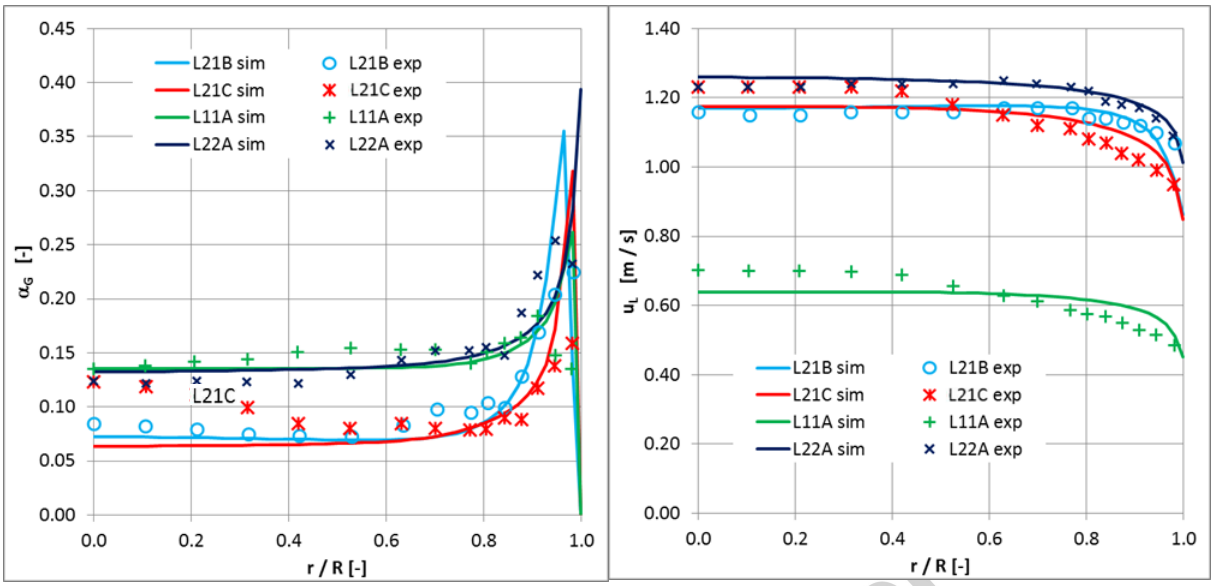

Figure 3: Gas volume fraction (a), axial liquid velocity (b), and turbulent kinetic energy (c) for the tests of Liu (1998). Solid lines: simulation results, symbols: measured values. The center of the column is on the left and the wall on the right of the plots.

Simulation results at the measurement level and experimental data for the four selected test conditions are shown in Fig. 3.
Part a) gives a comparison of the simulated and measured gas fraction profiles. In the center of the pipe the agreement between simulation and experiment is good except for case L21C. In this case the measured gas fraction profile has an additional center peak which is missed in the simulations. A likely cause for this peak is the existence of a fraction of bubbles with size

ACCEPTED MANUSCRIPT

larger than 6 mm, for which according to section 2.1.2 the lift force is directed towards the pipe center rather than towards the wall. This effect is missed by the monodisperse approximation. However due to the lack of detailed data on the bubble size distribution it is not possible to further examine this hypothesis. The gas fraction peak near the wall is overestimated by the simulations for all four test cases. A likely cause for this discrepancy is the neglect of bubble deformation due to contact with the wall.

Part b) gives a similar comparison for the axial liquid velocity. Near the pipe wall the simulated profiles have a gradient that is systematically too large. This corresponds with the overestimated wall peak in the gas-fraction a consequence of which is a too strong buoyant forcing of the liquid near the wall. Nonetheless, the relative deviation between simulation results and experimental data are small for all cases throughput the pipe.

In part c) finally the square root of turbulent kinetic energy is shown as a measure for the turbulent velocity fluctuations. As the present understanding of turbulence is limited even for single phase flows it is not surprising that the simulation results here show higher deviations from the measured data. Still the model predictions are reasonably close to provide useful estimates. In the center of the pipe the simulations tend to give larger values than measured while near the wall they tend to lower ones. An exception to this rule is again case L21C with the double peaked gas-fraction profile. For this particular set of tests the agreement could be improved by changing the value of the unknown coefficient $C_{\varepsilon B}$ in Eq. (15) but as shown in Rzehak and Krepper (2013b) this will degrade the predictions for other test cases. Thus with a view towards truly predictive applications where no data are available for comparison, we stick with the suggested value of $C_{\varepsilon B} = 1$ and accept a certain error.

In summary, a better treatment of the wall region and an improved turbulence modelling would be desirable, but knowing the error margins it is already possible to obtain useful engineering estimates from the simulations.

3.2 Bubble Column Test Case

The experiments of bin Mohd Akbar et al. (2012) were conducted in a flat bubble column of width D = 240 mm and a depth of 72mm using air and water at ambient conditions. Without gas supply the water level was at 0.7 m. Profiles of gas volume fraction, axial liquid velocity, and axial turbulence intensity as well as the bubble size distribution were measured at a level H = 0.5 m above the inlet. An electrical conductivity probe was used to measure gas fraction. The bubble size distribution was obtained by high-speed videometry. Liquid velocity and turbulence were measured by laser-Doppler-velocimetry.

The bubble size distribution was measured also near the inlet and no significant change was found compared with the measurement level. The mean bubble size calculated from the measured distributions is shown in Table 1. Two values of superficial gas velocities are available. For the lower one, all bubbles are smaller than 6 mm so that a monodisperse approximation suffices. For the higher gas flux in contrast a significant fraction of the bubbles is larger than 6 mm and the fixed polydisperse approximation with two groups is used. The measured bubble size distribution is thus represented by a small bubble group with a diameter of 5.3 mm containing 63 % of the total gas volume and a large bubble group with a diameter of 6.3 mm containing 37 % of the total gas volume.

Accepted manuscript

ACCEPTED MANUSCRIPT

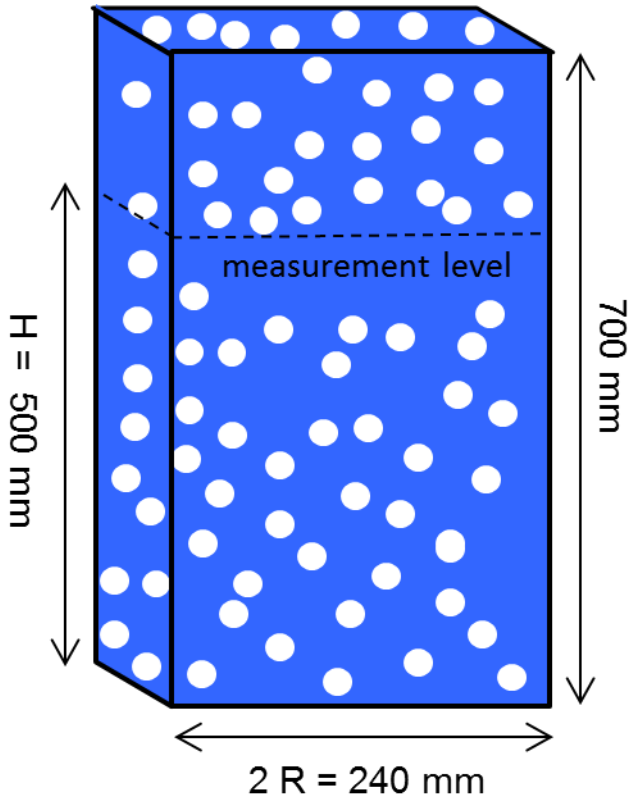

Figure 4: Sketch of the computational domain for the test cases of bin Mohd Akbar et al. (2012).

Fully 3D simulations on the domain sketched in Fig. 4 were run in transient mode. The resulting data were averaged over a sufficiently long period to obtain stationary averages. The change in the water level due to the gas is small enough not to affect the flow at the measurement level and was hence neglected. At the top of the column a degassing condition was prescribed. The sparger consists of 35 needles each of which which was modeled by an inlet area of approximately the size of the bubbles. The grid-spacing was 4.0 mm in all directions. Adaptive time-stepping was applied such that the Courant-Friedrichs-Lewy number remained below a value of one.

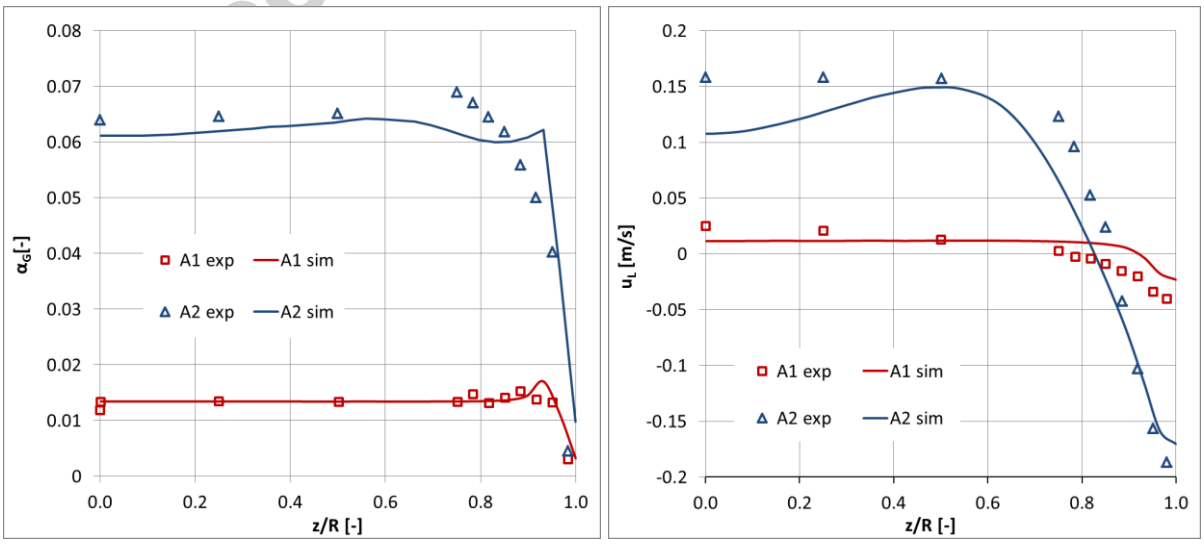

ACCEPTED MANUSCRIPT

a) b)

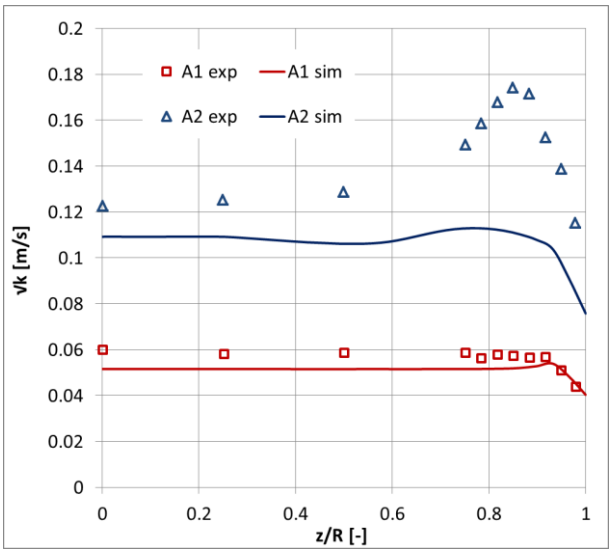

c)

Figure 5: Gas volume fraction (a), axial liquid velocity (b), and turbulent kinetic energy (c) for the tests of bin Mohd Akbar et al. (2012). Solid lines: simulation results, symbols: measured values. Only half of the column is shown with the center on the left and the wall on the right of the plots.

Results of the simulations for both of the available test conditions are shown in Fig. 5 in comparison with the experimental data. All of these data are taken on the mid-plane of the column.

Part a) gives the gas-fraction profiles. As before the agreement between simulation and experiment is excellent in the center of the column (z = 0). Near the wall (z = R) tiny peaks are seen in the simulated profiles which are absent in the measured ones. This is reminiscent of the overpredicted wall peaks in the pipe flow tests of section 3.1 although the quantitative deviation here is only minor.

Profiles of axial liquid velocity are given in part b). Here for both cases the simulated values of the upward flow in the center of the column are somewhat too low compared with the measured ones. Near the wall there is a recirculation directed downwards which again tends to be too small in magnitude in the simulations. Probably the most significant deviation between simulation and experiment is the point where the velocity becomes zero. This point is too close to the wall for the lower value of the gas flux and too close to the center for the higher value. For case A2, the simulated velocity profile shows a maximum that is not present in the measured data. As discussed by Ziegenhein et al. (2015), this maximum is related to the presence of a fraction of bubbles with size larger than 6 mm, for which according to section 2.1.2 the lift coefficient becomes negative. This leads to a potentially unstable situation: a local accumulation of these large bubbles, due to buoyancy and drag, causes a local maximum in the liquid velocity and this in turn by the action of the lift force, which is directed towards the highest liquid velocity, increases the accumulation of the large bubbles (Lucas et al., 2005). The resulting instability is counteracted by turbulent dispersion. The mismatch between experiment and simulation thus points to the fact that the balance between lift and turbulent dispersion is not described perfectly by the model.

Part c) finally shows the square root of turbulent kinetic energy as a measure for the turbulent velocity fluctuations. It should be noted that as discussed in detail in Ziegenhein et al. (2015)

Accepted manuscript

ACCEPTED MANUSCRIPT

this quantity here is composed of two contributions, one from the modeled k and one from the variance of the time-dependent liquid velocity. In the center of the column the simulated values are only slightly smaller than the measured ones for both test cases. Near the wall a good match is obtained for the lower gas flux while for the higher gas flux the peak seen in the experimental data is missed by the simulations.
In summary, particularly the turbulence modeling is seen to deserve further improvement, but again the overall agreement between simulation and experiment is quite good already.

3.3 Airlift Column Test Case

Data on air / water bubbly flow in an internal loop airlift column have been presented by Luo (2005). In the following that part of these data that will be used for comparison with our simulations is described. The column consists of a round container with 130 mm inner diameter into which a 1050 mm long draft tube of 80 mm inner diameter and 5 mm wall thickness is inserted. The distance of the lower end of the draft tube from the bottom of the column is 50 mm. The distance of the upper end of the draft tube from the static water level, i.e. the water level without any gas present, is 30 mm. Gas is supplied through a ring sparger of 25 mm inner diameter located 25 mm above the column bottom and made of a tube with 5 mm outer diameter. The average gas volume flux through the entire cross section of the container is J_G = 0.01 m/s. A total gas hold-up of ~3% has been measured. From this, the dynamic water level is calculated as 1160 mm.
Two types of measurement have been performed. Radial profiles of the time-averaged gas fraction have been measured by γ-ray tomography at five different heights in column. Only the central height at 677 mm will be used in the present comparison. The liquid velocity has been determined by Computer-Automated Radioactive Particle Tracking (CARPT). Radial profiles of both the time-averaged axial velocity and turbulent kinetic energy are available. These values represent averages over the range between 300 and 800 mm column height. The density of the tracer particle has been matched to that of the water used as carrier liquid but due to the rather large size of the particle (0.8 mm diameter) some deviation between the true liquid velocity and the measured velocity of the tracer particle may still exist

Accepted manuscript

ACCEPTED MANUSCRIPT

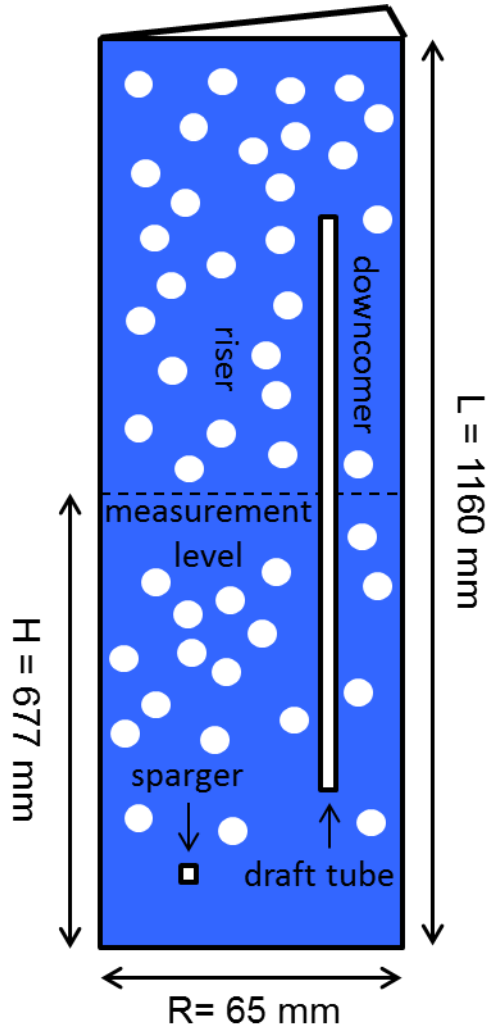

Figure 6: Sketch of the computational domain for the test cases of Luo (2005).

For the bubble size a value of 3 mm is given, but it is not explained how this value has been obtained, so that it can only be considered as a rough estimate. It must be noted that in particular simple inspection of the column from the outside may give grossly wrong results for the average bubble size. For example lift forces (see section 2.1.2) may result in a tendency of smaller bubbles to accumulate near the walls while larger bubbles are depleted in this region. Especially in the downcomer which is seen from the outside only the smaller bubbles are expected because the larger bubbles in the riser likely exit the column immediate when reaching the top. Since the origin of the reported value is not known and its reliability cannot be judged, the bubble size will be treated as a parameter in the simulations. To avoid introducing more than one parameter the monodisperse approximation is used although the flow in reality is likely to be polydisperse.

For the geometry, a quasi-2d domain corresponding to a narrow sector of the column is used together with axisymmetric conditions. The draft tube and sparger are cut out from the domain as sketched in Fig. 6. The rise of the water level due to the gas strongly affects the distance to the top end of the draft tube and hence dynamic height is taken for the computational domain. The gas mass flux was specified on the top surface of the sparger. At the top of the domain a degassing condition was imposed. The calculations were made in transient mode because in stationary mode convergence problems occurred. The grid spacing was 2.5 mm in the radial direction. In the axial direction a grid spacing of 2.5 mm was used

Accepted manuscript

ACCEPTED MANUSCRIPT

for the bottom and top parts while the central part used a coarser mesh with a spacing of 20 mm (see Liao et al. 2016 for details). Adaptive time-stepping was applied such that the Courant-Friedrichs-Lewy number remained below a value of one.

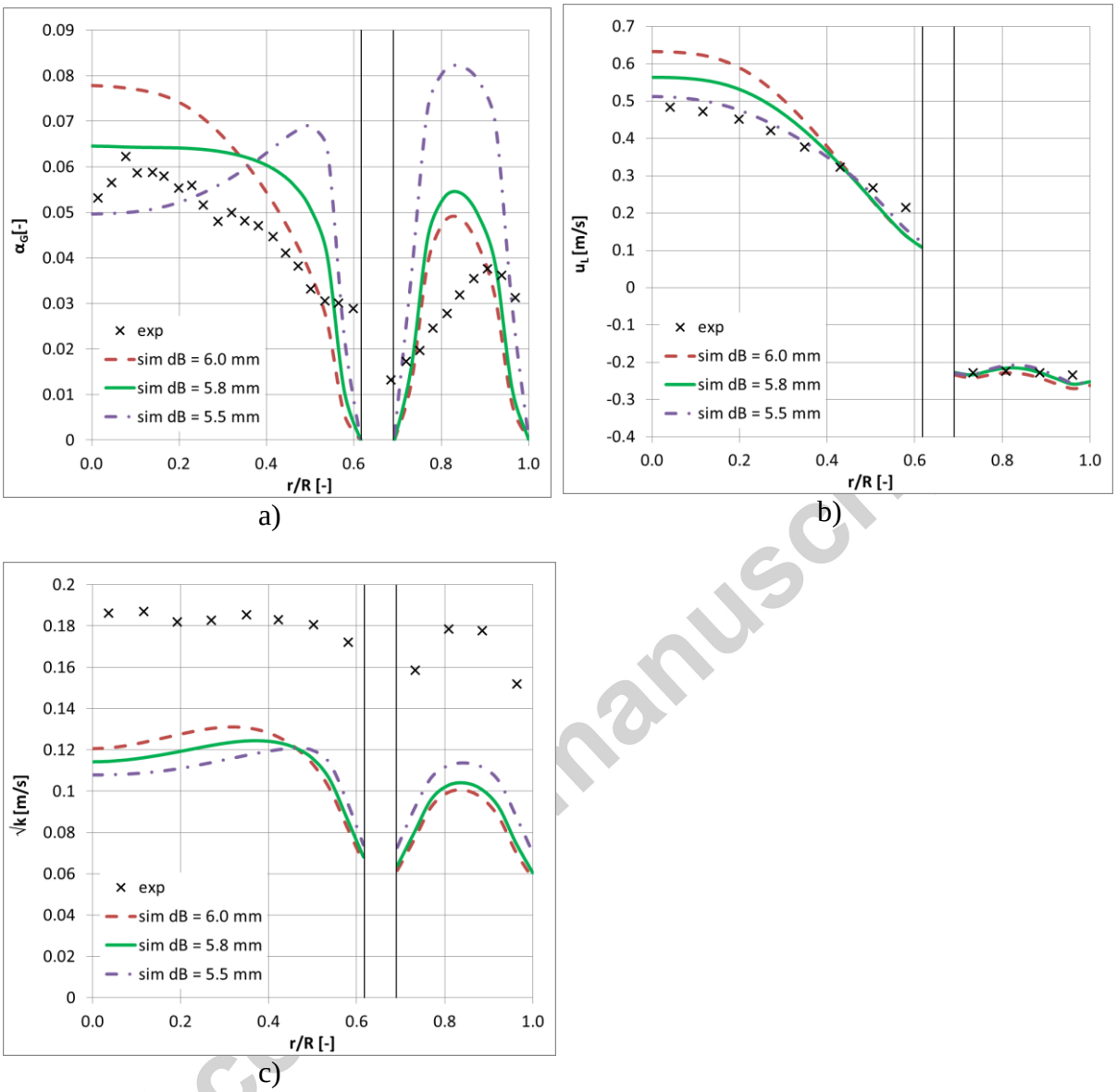

Figure 7: Gas volume fraction (a), axial liquid velocity (b), and turbulent kinetic energy (c) for the tests of Luo (2005). Note that results for the latter two quantities represent averages over the range between 300 and 800 mm column height. Lines: simulation results, symbols: measured values. Different values have been used for the bubble size, namely d_B = 5.5 mm (dash-dotted), d_B = 5.8 mm (solid), and d_B = 6.0 mm (dashed). The center of the pipe is on the left and the wall on the right of the plots. The position of the draft tube is indicated by the vertical lines.

Results of the simulations (lines) are compared with the experimental data (symbols) in Fig. 7. Since no reliable measurement is available for the bubble size, three values have been

ACCEPTED MANUSCRIPT

considered, namely d_B = 5.5 mm (dash-dotted), d_B = 5.8 mm (solid), and d_B = 6.0 mm (dashed).

Part a) shows the profiles of the gas fraction. For d_B = 5.5 mm the simulations give a wall peaked profile in the riser, while for d_B = 5.8 mm and d_B = 6.0 mm a center peaked profile is obtained. Clearly only the latter matches with the experimental data. In addition the simulated gas fraction in the downcomer is much farther away from the measurement for d_B = 5.5 mm than for d_B = 5.8 mm and d_B = 6.0 mm. Therefore it is likely that the true average bubble size is in the range around 5.8 to 6.0 mm rather than 3.0 mm as reported in Luo (2005), although some deviations are seen also for the simulations with d_B = 5.8 or 6.0 mm. Since these values are close to the sign change in the lift force as described in section 2.1.2 a simulation with fixed polydispersity distinguishing two groups of larger and smaller bubble would be more appropriate. However, in the absence of measured bubble size distributions to determine appropriate group diameters and group fractions there are too many unknowns to carry this approach through.

One may note that there appears to be a close correspondence between the amount of gas within a zone of roughly one third of the radius next to the draft-tube wall within the riser and the amount of gas that is drawn into downcomer. This suggests that bubbles near the draft-tube wall are carried over to the downcomer, while those in the center of the riser escape through the free surface at the top of the column. An accurate representation of the gas fraction profile in the riser thus is a key issue for the modelling.

Axial liquid velocities are shown in part b). The influence of the value chosen for the bubble size is only small here and a reasonable match with the experimental data is obtained for all values considered both in the riser and in the downcomer.

Finally part c) gives the square root of turbulent kinetic energy as a measure for the turbulent velocity fluctuations. Again the influence of the value chosen for the bubble size is only small. The shape of the simulated profiles is similar to that of the measured ones but the values are about a factor of two too small. As discussed for the pipe flow tests in section 3.1 the agreement for this particular test could be improved by changing the value of the unknown coefficient $C_{\varepsilon B}$ in Eq. (15) but we rather maintain general applicability of the model and accept the error which for turbulence is not quite that bad.

In summary, once again turbulence modeling is seen to deserve improvement the most but as before overall the agreement between simulation and experiment is of engineering quality already. It may be added that the inclusion of precise measurements of bubble size and preferably its distribution is highly desirable for data that are used to validate simulation models.

Accepted manuscript

4 DISCUSSION AND CONCLUSIONS

A previously proposed baseline closure model for bubbly flows has been applied to a number of different geometries and boundary conditions. In particular bubbly pipe flow, a bubble column and an airlift column have been considered which also vary in cross-sectional shape and dimension. The model has been found capable to reproduce experimental data for all cases with a similar accuracy that is useful for engineering design estimations. The possibility of such a unified description may be expected since the physical phenomena on the scale of individual bubbles which are described by the closure relations is the same for all cases. An explicit demonstration as given here, however, has not been shown before.

A full validation of models like the one presented here demands high quality experimental data which provide in particular low measurement errors, good spatial resolution, and a large

ACCEPTED MANUSCRIPT

set of observed quantities. Among the latter, the bubble size is of utmost importance to know, since it appears in all of the correlations used. The data employed in the present study meet this last requirement to different degrees. Measurements of the full distribution of bubble sizes are available only for the bubble column data of bin Mohd Akbar et al. (2012), the mean bubble size has been measured by Liu (1998) for pipe flow, but only an uncertain estimate is known for the airlift column of Luo (2005). Therefore, in the last case, bubble size has been treated as an adjustable parameter to illustrate the potential of the modelling approach. We actively pursue the goal to close the gap to a full validation by new experiments which include precise measurements of the bubble size distribution (Ziegenhein et al. 2016).

Of course also the accuracy reached by the model prediction leaves room for improvement. To get a fair judgement one may look at other works in the literature that have considered the same test cases individually.

Test L21C of Liu (1998) was also simulated by Troshko and Hassan (2001) (named L7 in their paper) using a monodispersed Euler-Euler model. In the bubble forces constant lift coefficient was used and a different expression for the turbulent dispersion force. Turbulence was described by a plain k-ε-model with a different bubble-induced turbulence source term in the ε-equation. Quantitatively the agreement they obtained is very similar to ours.

Bin Mohd Akbar et al. (2012) also presented simulation along with their experiments. They used a polydisperse Euler-Lagrange model with LES treatment for the turbulence. Slightly different correlations were applied for the bubble forces while bubble-induced turbulence is neglected. Again the quantitative agreement they reached is similar to ours with slightly better accuracy for the liquid velocity.

Luo (2005) also gave simulations for the test considered here applying a monodisperse Euler Euler approach with a plain k-ε turbulence model. For the bubble-induced turbulence no source terms were added to the turbulence equations but a contribution to the turbulent viscosity was considered. Different models were tested for the bubble forces. The one that is most similar to ours has no lift force and a different model for the turbulent dispersion force.

Different from our study they assumed a bubble size of 3 mm. The results obtained with this setup (see their Figure 6-6) give a better match for the gas fraction in the downcomer which is overestimated in our results, and somewhat improved accuracy for the liquid velocity in the riser. Otherwise similar results are found.

Luo (2005) also investigated the influence of a Saffman-lift force and concluded that best results are obtained in the absence thereof (see their Figure 6-8). In this context it should be noted that Saffmann's (1965, 1968) treatment applies to spherical particles and does not consider effects of deformation which according to the experiments of Tomiyama et al. (2002) are dominant for bubbles. Therefore this conclusion should be considered with care. In addition a precise measurement of bubble size may be needed to make a definite assessment of the importance of the lift force since this force depends strongly thereon.

In conclusion, other treatments using somewhat different sets of closure relations may improve accuracy for isolated aspects. However, the accuracy achieved by the baseline model used here is not much worse and in a range that is useful for engineering purposes. As a rough guide it may be said that typical deviations between measured and simulated data are in the range of 20-30% for the void fraction and mean liquid velocity and in the worst case up to a factor of 2 for the turbulent fluctuations.

The benefit of having a unified model that works for a large range of applications becomes obvious when true predictions are sought. In this situation all modelling decisions must be made beforehand and no data on the problem at hand are available for comparison. Knowing that the baseline model has worked for a number of similar applications makes it a robust choice for such applications.

Accepted manuscript

ACCEPTED MANUSCRIPT

Some limitations of the model in its present form deserve discussion together with possibilities for their improvement.

First of all, swarm effects, i.e. dependencies of the coefficients in drag, lift, and other forces on the gas fraction, have been neglected. In particular, when higher local gas fractions occur, a better accuracy may be expected if these effects are included. For the drag force, some further results are available from the literature (e.g. Roighair et al. 2011). For the other forces, literature results are insufficient for this purpose. Direct numerical simulations of small groups of bubbles have recently become available as a tool which is well suited to fill this gap.

A second limitation arises from the use of the two-equation SST-model for turbulence which is isotropic and rests on the Boussinesq hypothesis. Extension to a full Reynolds-stress model is a promising line for improvement in this direction. From studies of singlephase flows it is known that such a model is capable to capture anisotropies, describe secondary flows of Prandtl's second kind and include effects of streamline curvature and rotation. The challenge in the adaptation to multiphase flows will be the development of suitable anisotropic source terms for the bubble-induced turbulence.

Finally, the inclusion of processes of bubble coalescence and breakup would be highly desirable. Attempts in this direction have already been made (e.g. Liao et al. 2015), but have not yet reached a state that would allow engineering predictions to be made. As already mentioned above, high quality data for model validation are needed to this end which include in particular precise measurements of the bubble size distribution.

5 ACKNOWLEDGEMENT

This work has been carried out in the frame of a research project (GZ: RZ 11/1-1) within the DFG Priority Programme 1740: "Reactive Bubbly Flows" funded by the DFG.

6 NOMENCLATURE

Notation	Unit	Denomination
A_I	-	Interfacial area density
C_B ((1981_Sato) model)	-	bubble-induced turbulence coefficient
C_D	-	drag coefficient
C_L	-	lift coefficient
C_{TD}	-	turbulent dispersion coefficient
C_{VM}	-	virtual mass force coefficient
C_W	-	wall force coefficient
C_μ	-	shear-induced turbulence coefficient (k-ε model)
d_B	m	bubble diameter (volume equivalent sphere)
$d_\perp$	m	bubble diameter perpendicular to main motion
D	m	pipe or column diameter / width
Eo	-	Eötvös Number
F_D	N m^{-3}	drag force
F_L	N m^{-3}	lift force
F_{TD}	N m^{-3}	turbulent dispersion force
F_{VM}	N m^{-3}	virtual mass force

Accepted manuscript

ACCEPTED MANUSCRIPT

F_W	N m^{-3}	wall force
g	m s^{-2}	acceleration of gravity
G	kg s^{-1} m^{-2}	mass flux
H	m	measurement position
J	m s^{-1}	volumetric flux = superficial velocity
k	m^2 s^{-2}	turbulent kinetic energy
L	m	length of domain
Mo	-	Morton Number
p	Pa	pressure
r	m	radial coordinate
R	m	pipe or column radius / half-width
Re	-	Reynolds number
s	m	hydrodynamic wall roughness
t	s	time
u	m s^{-1}	velocity
u_τ	m s^{-1}	friction velocity
U	m s^{-1}	velocity scale
V	m^3	volume
x	m	axial coordinate
y	m	distance to the wall
z	m	spanwise coordinate
α	-	volume fraction
δ	m	viscous length scale
ε	m^2 s^{-3}	turbulent dissipation rate
μ	kg m^{-1} s^{-1}	dynamic viscosity
ν	m^2 s^{-1}	kinematic viscosity
ρ	kg m^{-3}	density
σ	N m^{-1}	surface tension
τ_W	N m^{-2}	wall shear stress

7 REFERENCES

ANSYS, 2012. ANSYS CFX-Solver Theory Guide Release 14.5. ANSYS Inc.

Auton, T., Hunt, J., and Prud'Homme, M., 1988. The force exerted on a body in inviscid unsteady non-uniform rotational flow. Journal of Fluid Mechanics 197, 241.

Burns, A.D., Frank, T., Hamill, I., and Shi, J.-M., 2004. The Favre averaged drag model for turbulence dispersion in Eulerian multi-phase flows, Proc. 5th Int. Conf. on Multiphase Flow, ICMF2004, Yokohama, Japan, 2004.

Drew, D. A., and Passman, S. L., 1998. Theory of Multicomponent Fluids, Springer.

Dudukovic, M. P., 2010. Reaction engineering: Status and future challenges. Chemical Engineering Science 65, 3.

Frank, T., Zwart, P., Krepper, E., Prasser, H.-M. and Lucas, D., 2008. Validation of CFD models for mono- and polydisperse air–water two-phase flows in pipes. Nuclear Engineering and Design 238, 647.

Accepted manuscript

ACCEPTED MANUSCRIPT

Hosokawa, S., Tomiyama, A., Misaki, S. and Hamada, T., 2002. Lateral Migration of Single Bubbles Due to the Presence of Wall, Proc. ASME Joint U.S.-European Fluids Engineering Division Conference, FEDSM 2002, Montreal, Canada.

Ishii, M., and Hibiki, T., 2011 Thermo-fluid dynamics of two-phase flow. Springer, 2nd ed.

Ishii, M., and Zuber, N., 1979. Drag coefficient and relative velocity in bubbly, droplet or particulate flows, AIChE Journal 25, 843.

Jakobsen, H. A., Lindborg, H., and Dorao, C. A., 2005. Modeling of bubble-Column Reactors: Progress and Limitations. Industrial and Engineering Chemistry Research 44, 5107.

Joshi, J. B., 2001. Computational flow modelling and design of bubble column reactors. Chemical Engineering Science 56, 5893.

Joshi, J. B., and Ranade, V. V., 2003. Computational Fluid Dynamics for Designing Process Equipment: Expectations, Current Status, and Path Forward. Industrial and Engineering Chemistry Research 42, 1115.

Kataoka, I., Besnard, D. C. and Serizawa, A., 1992. Basic Equation of Turbulence and Modeling of Interfacial Transfer Terms in Gas-liquid Two-phase Flow. Chemical Engineering Communications 118, 221.

Krepper, E., Lucas, D., Frank, T., Prasser, H.-M. and Zwart, P., 2008. The inhomogeneous MUSIG model for the simulation of polydispersed flows. Nuclear Engineering and Design 238, 1690.

Liao, J., Ziegenhein, T., and Rzehak, R., 2016. Bubbly flow in an airlift column: a CFD study. Journal of Chemical Technology & Biotechnology, in press, DOI: 10.1002/jctb.4917.

Liao, Y., Rzehak, R., Lucas, D. and Krepper, E. , 2015. Baseline Closure Model for Dispersed Bubbly Flow: Bubble-Coalescence and Breakup. Chemical Engineering Science 122, 336.

Liu, T. J., 1998. The role of bubble size on liquid phase turbulent structure in two-phase bubbly flow. 3rd Int. Conf. on Multiphase Flow, ICMF1998, Lyon, France.

Lucas, D., Prasser, H.-M., Manera, A., 2005. Influence of the lift force on the stability of a bubble column. Chemical Engineering Science 60, 3609.

Lucas, D. and Tomiyama, A. , 2011. On the role of the lateral lift force in poly-dispersed bubbly flows. International Journal of Multiphase Flow 37, 1178.

Luo, H.-P., 2005. Analyzing and Modeling of Airlift Photobioreactors for Microalgal and Cyanobacteria Cultures. PhD-thesis, Washington University, St. Louis.

Magnaudet, J., Rivero, M., and Fabre, J., 1995. Accelerated flows past a rigid sphere or a spherical bubble Part 1: Steady straining flow. Journal of Fluid Mechanics 284, 97.

Maxey, M. R., and Riley, J. J., 1983. Equation of motion for a small rigid sphere in a nonuniform flow. Physics of Fluids 26, 883.

Accepted manuscript

ACCEPTED MANUSCRIPT

Menter, F., 1994. Two-equation eddy-viscosity turbulence models for engineering applications, AIAA Journal 32, 1598.

Menter, F. R., 2009. Review of the shear-stress transport turbulence model experience from an industrial perspective. International Journal of Computational Fluid Dynamics 23, 305.

bin Mohd-Akbar, M., Hayashi, K., Hosokawa, S., and Tomiyama, A., 2012. Bubble tracking simulation of bubble-induced pseudoturbulence. Multiphase Science and Technology 24, 197.

Ranade, V. V., 1995. Computational fluid dynamics for reactor engineering. Reviews in Chemical Engineering 11, 229.

Roghair, I., Lau, Y., Deen, N., Slagter, H., Baltussen, M., Van Sint Annaland, M., and Kuipers, J., 2011. On the drag force of bubbles in bubble swarms at intermediate and high Reynolds numbers. Chemical Engineering Science 66, 3204.

Rzehak, R., Krepper, E. and Lifante, C., 2012. Comparative study of wall-force models for the simulation of bubbly flows. Nuclear Engineering and Design 253, 41.

Rzehak, R., and Krepper, E., 2013a. Closure models for turbulent bubbly flows: A CFD study. Nuclear Engineering and Design 258, 265, 701.

Rzehak, R., and Krepper, E., 2013b. CFD modeling of bubble-induced turbulence. International Journal of Multiphase Flow 55, 138.

Rzehak, R., and Krepper, E., 2015. Bubbly flows with fixed polydispersity: validation of a baseline closure model. Nuclear Engineering and Design 287, 108.

Saffman, P. G., 1965. The lift on a small sphere in a slow shear flow. Journal of Fluid Mechanics 22, 385.

Saffman, P. G., 1968. Corrigendum to "The lift on a small sphere in a slow shear flow". Journal of Fluid Mechanics 31, 624

Schmidtke, M., 2008. Investigation of the dynamics of fluid particles using the Volume of Fluid Method. PhD-Thesis, University Paderborn, (in German).

Tomiyama, A., Sou, A., Zun, I., Kanami, N. & Sakaguchi, 1995. Effects of Eötvös number and dimensionless liquid volumetric flux on lateral motion of a bubble in a laminar duct flow. Proc. 2nd Int. Conf. on Multiphase Flow, Kyoto, Japan, 3.

Sundaresan, S., 2000. Modeling the Hydrodynamics of Multiphase Flow Reactors: Current Status and Challenges. AIChE Journal 46, 1102.

Tomiyama, A., Kataoka, I., Zun, I., and Sakaguchi, T., 1998. Drag Coefficients of Single Bubbles under Normal and Micro Gravity Conditions. JSME International Journal B 41, 472.

Tomiyama, A., Tamai, H., Zun, I., and Hosokawa, S., 2002. Transverse migration of single bubbles in simple shear flows, Chemical Engineering Science 57, 1849.

Troshko, A. A., and Hassan, Y. A., 2001. A two-equation turbulence model of turbulent bubbly flows. International Journal of Multiphase Flow 27, 1965.

Wellek, R.M., Agrawal, A.K., and Skelland, A.H.P., 1966. Shapes of liquid drops moving in liquid media. AIChE Journal 12, 854.

Accepted manuscript

ACCEPTED MANUSCRIPT

Wilcox, D. C., 1998. Turbulence Modeling for CFD. DCW-Industries.

Yeoh, G. H., and Tu, J. Y., 2010. Computational Techniques for Multiphase Flows — Basics and Applications, Butterworth-Heinemann, Elsevier Science and Technology.

Ziegenhein, T., Rzehak, R., and Lucas, D., 2015. Transient simulation for large scale flow in bubble columns. Chemical Engineering Science 122, 1.

T. Ziegenhein, J. Zalucky, R. Rzehak, and D. Lucas, 2016. On the hydrodynamics of airlift reactors, Part I: Experiments. Chemical Engineering Science, submitted.

Zun, I. 1980. The transverse migration of bubbles influenced by walls in vertical bubbly flow. International Journal of Multiphase Flow 6, 583.

Highlights

- a closure model for bubbly flow is proposed
- including bubble forces and bubble-induced turbulence
- it allows to treat different geometries and boundary conditions in a unified manner
- specifically bubbly flow in a pipe, a bubble column and an airlift column are considered

Accepted manuscript